Available online at
www.ijacskros.com

Indian
Journal of Advances in
Chemical Science

Indian Journal of Advances in Chemical Science 2 (2014) 36-41

Determination of Stacking Faults and Micro Structural Parameters in PVA/ZnO Nanocomposite Films using Whole Pattern Fitting Technique.

K.S. Prashanth[1], S.S. Mahesh[2], B. M. Nagbhushana[3], M.B. Nanda Prakash[4], R. Somashekar[4]*

[1]*Department of Physics, New Horizon College of Engineering, Bangalore, Karnataka, India 560103.*
[2]*Department of Physics, Acharya Institute of Technology, Bangalore, Karnataka, India, 560 107.*
[3]*Department of Chemistry, M S Ramiah Institute of Technology, Bangalore, Karnataka, India.*
[4]*Department of Studies in Physics, University of Mysore, Manasagangotri, Mysore, Karnataka, India570006.*

Received 2nd April 2014; Accepted 20th April 2014.
Editor in Chief: Dr. K.S.V. Krishna Rao; Guest Editors: Dr. Siddaramaiah, Dr. G. M. Shashidhara.
Presented at the POLYCON-2014, 6th National Conferences on Advances in Polymeric Materials [Energy, Environment & Health] (NCAPM), Mysore, India, 25-26 April 2014.

ABSTRACT:

A series of poly(vinyl alcohol) (PVA)/ZnO films were cast. The synthesized PVA/ZnO films with various weight percentages 0wt%, 1wt%, 2wt%, 3wt% were subjected to XRD analysis for the characterization process for estimating the size of crystalline particle. Zinc Oxide Nanoparticles were synthesized by solution combustion method employing ODH as fuel with corresponding metal nitrate. The crystallite size (<N>), lattice strain (g in %), stacking faults (α_d) and twin faults (β) were determined by whole powder pattern fitting technique, developed by us. We have studied the microcrystalline parameters from XRD. Activation energy has been computed for these systems.

***Key Words**: Stacking and Twin faults, Micro structural parameters, Solution combustion method, Nano composite*

1. INTRODUCTION

Metal and Metal Oxide nanoparticles as fillers into Polymer matrix demonstrate remarkably improved properties with respect to the pure polymers. Polymeric Nano composites exhibits improved mechanical properties such as Tensile strength, YoungsModulus, Thermal Conductivity, Film barrier properties, Drug solubilization properties [1-5]. ZnO is also considered as Biocompatible, innoxious catalyst, suitable for various photo catalytic reactions. ZnO is propitiousmaterial for Gas sensors, UV absorbers, Food Packaging, Solar Cells, and Bio-Medical applications [6-10]. Poly(vinyl alcohol) (PVA) is an ecofriendly polymer due to its biodegradability [11].

The Extensive studies have been reported in the literature on the influence of zinc oxide nanoparticles on ZnO/PVA films. Dielectric loss tangent (tan δ) decreases with increase in filler content at lower frequency, but at higher frequencies the tan δ increases with increase in nanoparticles concentration in ZnO-Ce_2O_3/PVA Nano composite films [12]. Flame Retardancy[13] of the poly(vinyl alcohol)-ZnO Nano composites in which ZnO have barrier effect to slow down the product volatilization and thermal transport during decomposition of the polymer have been reported.Similarly presence of 20% of nano-cellulose particles from linen in the PVA matrix increases the mechanical properties, such as tensile strength and percentage elongation at break. Higher percent of the nano-cellulose particles decreases the tensile strength due to the change in the morphological structure of the PVA film [14]. Thorough research has been carried out on Nanoparticles of uncapped and poly(vinyl alcohol) capped zinc oxide which revealed the reduced photocatalytic activity of PVA capped ZnO. [15,16].

In this study the Zinc oxide nanoparticles were synthesized via Solution combustion process usingoxalyl di-hydrazide as fuel and PVA/ZnO/NaCl polymer blends were prepared by Solvent cast method. The crystallite size (<N>), lattice strain (g in %), stacking faults (α_d) and twin faults (β) were determined by whole powder pattern fitting technique, developed by us using XRD data.

**Corresponding Author: R Somashekar: rs@physics.uni-mysore.ac.in*

2. EXPERIMENTAL

2.1. Materials and Methods

2.1.1. Synthesis of Zinc Oxide Nanoparticles

Zinc nitrate [$Zn(NO_3)_2$,$6H_2O$] acted as an oxidizing reactant and oxalyl di-hydrazide (ODH) [$C_2H_6N_4O_2$] as a reducing one.The Stoichiometric ratio of mixture was taken in borosilicate petri dish and stirred for few minutes and later it was introduced into Muffle furnace maintained at 300^0C.The Mixture undergoes thermal dehydration with the liberation of large amount of gases with very high flame temperature. The entire combustion process is accomplished in less than 5 min.

2.1.2. Preparationof PVA/NaCl/ZnONano composites

PVA/NaCl-ZnONano composites were prepared by solution casting method.PVA was dissolved in distilled water by heating at 60^0 C for 16 h under stirring.This was used as stock solution 0 wt% .The blends with varying amounts viz., 1wt%,2wt%,3wt% and 4 wt% of Nacl and 0.1wt%,0.2wt%,0.3wt%and 0.4wt% of ZnO nanoparticles were prepared by stirring the appropriate weight percentages of the blends for 30 min and the films were cast from blend The PVA/NaCl -ZnO solution was casted on to a cleaned glass plate and dried at room temperature.

2.2. Theory

The contribution of crystallite size, lattice strain and stacking faults[17] to a Bragg reflection profile can be written as,

$$I_{hkl}(s_{hkl}) = \int_{-\infty}^{\infty} T^{IP}(nd) e^{[2\pi i\zeta(nd)]} e^{[2\pi i\phi(nd)]} e^{[2\pi i nd s_{hkl}]} d(nd) \quad (1)$$

where $I_{hkl}(s_{hkl})$ is the intensity of a profile in the direction joining the origin to the center of the reflection, T^{IP} is the Fourier transform of instrument profile, $e^{[2\pi i\zeta(nd)]}$ is the average phase factor due to lattice distortion(ζ) and $e^{[2\pi i\varphi(nd)]}$ is due to crystallite size / stacking faults(φ). L = nd (with $d=d_{hkl}$) is the column length. Equation (1) can be written in the form of Fourier series as,

$$I_{hkl}(s_{hkl}) = \sum_{n=-\infty}^{\infty} A_{hkl}(n)\cos\{2\pi n d_{hkl}(s-s_0)\} \quad (2)$$

where$A_{hkl}(n)$ are corrected Fourier coefficients with Fourier coefficients of instrumental profile function $T^{IP}(nd)$, s is $\sin\theta/\lambda$ and s_0 is the value of s at the peak of the reflection. Here afterwards, we refer to crystallite size in terms of the average number of unit cells counted in a direction perpendicular to the Bragg plane (hkl) with a notation <N>, and the crystallite size in Å is given by $D_{hkl} = \langle N\rangle d_{hkl}$($d_{hkl}$ is the perpendicular spacing of the (hkl) planes from their origin). These Fourier coefficients $A_{hkl}(n)$ are functions of the size of the crystallite, the disorder of the lattice and stacking faults coefficients, i.e.

$$A_{hkl}(n) = A^s_{hkl}(n).A^d_{hkl}(n).A^F_{hkl}(n) \quad (3)$$

Fourier analysis of a Bragg reflection profile must always be performed [17] over the complete cycle of the fundamental form d ($s-s_o$) = -1/2 to +1/2, which is rarely possible experimentally. We do this analysis with the available truncated range by introducing truncated correction [18]. For a paracrystalline material, with Gaussian strain distribution, $A^d_{hkl}(n)$[17,19-20] turns out to be

$$A^d_{hkl}(n) = \exp(-2\pi^2 n^2 m g^2) \quad (4)$$

where m is the order of the reflection and g = ($\Delta d/d$) is the lattice strain. Normally one also defines mean square strain $\langle\varepsilon^2\rangle$ that is given by g^2/n. This mean square strain is dependent on n (or column length L = nd), whereas g is not. With exponential distribution function for column length, we have,

$$A^S_{hkl}(n) = \begin{cases} A(0)\left(1 - n/\langle N\rangle\right), & ;\text{if } n < p \\ A(0)\left\{\exp\left[-\alpha\,(n-p)\right]\right\}/(\alpha\,N) & ;\text{if } n \geq p \end{cases} \quad (5)$$

In the above equation $\alpha = 1/(N-p)$, refers to the width of the distribution and p is the smallest number of unit cells in a column.

The whole powder pattern of samples were simulated using individual Bragg reflections represented by the above equations using

$$I(s) = \sum_{hkl} (\omega_{hkl} I_{hkl} - BG) \quad (6)$$

whereω_{hkl} are the appropriate weight functions for the (hkl) Bragg reflection. Here s takes the whole range ($2\theta \approx 6^0$ to 60^0) of X-ray diffraction recording of the sample. BG is an error parameter introduced to correct the background estimations.

3. RESULTS AND DISCUSSION

X-ray diffraction pattern of Polymer blend film samples were recorded on RigakuMiniflex II Diffractometer with Ni filtered, CuK_α radiation of wavelength 1.542 Å, and a graphite monochromator. The scattered beam from the sample was focused on to a detector. The specifications used for the recording were 30 kV and 15 mA. The sample was scanned in the 2θ range of 6^0 to 60^0 with a scanning step of 0.02^0.

Figure 1shows the XRD of as-formed ZnO nano particles. The three strongest XRD peaks for ZnO were detected corresponding to Bragg angles

Table 1. Microstructural parameters and stacking faults for pure PVA and PVA doped Zinc using exponential distribution function.

Sample	2θ	d(Å)	N	D(Å)	g(%)	α	α^d	β	Delta	Crystallite area ($Å^2$)
PURE	19.67	4.52	8	36.18	0	0.909	2.82E-7	1.74E-4	2.86E-3	687.4
	41.27	2.18	8.7	19.00	0	3.206	6.02E-5	4.16E-6		
1%	19.50	4.54	6.8	30.92	0	0.483	3.45E-7	1.78E-4	1.06E-3	13190
	31.42	2.84	150	426.6	0	1.874	4.96E-6	1.09E-5		
	31.65	2.82	100	282.4	0	1.904	2.16E-5	2.11E-5		
	45.40	1.99	150	299.4	0	1.893	1.69E-5	2.12E-5		
2%	19.59	4.52	9	40.74	0	0.481	1.76E-5	1.05E-4	0.57E-3	20207
	31.72	2.81	140	394.5	0	1.748	7.89E-6	1.97E-5		
	45.69	1.98	250	496.0	0	0.612	4.21E-9	1.76E-9		
3%	18.8	4.71	8.5	40.08	0	0.314	2.43E-5	7.37E-5	0.92E-3	15150
	30.72	2.90	130	378.0	0	1.905	8.62E-6	9.94E-6		
	44.51	2.03	160	325.2	0	1.691	8.62E-6	9.98E-6		
4%	19.53	4.54	10.5	47.68	0	0.480	1.88E-5	1.90E-5	0.40E-3	14246
	31.74	2.81	85	239.3	0	1.899	1.20E-5	2.13E-5		
	45.49	1.99	150	298.8	0	1.676	9.47E-6	9.59E-6		

31.4◦, 34.1◦ and 36.2◦ respectively.All diffraction peaks are consistent with the standard PDF database (JCPDS file No. 89-511).with the hexagonal ZnO structure with lattice constants a=3.249(1) A˚ and c=5.2052(2)A˚ .Average particle size was estimated using Debye-Scherer formula given by

$$D = 0.9 \lambda / \beta \cos \theta \quad (7)$$

Where ,λ is the wavelength of X ray, β Full Width at Half Maximum (FWHM) , D is the particle size

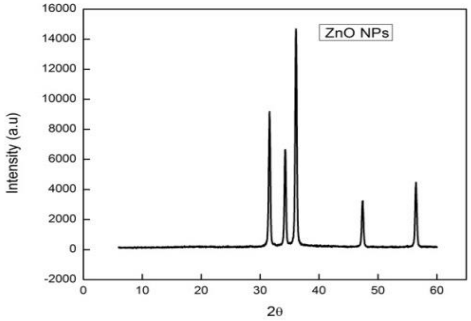

Figure1: XRD pattern of ZnO nanoparticles.

which was found to be around 24 nm.In the first step, the micro structural parameters were refined for individual profiles of X-ray recordings in each of the sample and the computed values of crystallite size <N>, lattice strain (g in %), stacking fault probability and twin fault probability are given in Table 1 for Pure PVA and PVA doped with various weight percentages of Zinc Oxide nanoparticles and Sodium chloride salt using exponential column length distribution. We observe that the lattice strain in both is 0.0% and average crystallite area in the PVA/ZnO Nano composite increases compared to Pure PVA. The Figure 2 shows the XRD pattern of Pure PVA andPVA/NaCl/ nano-ZnO/ composite film, which shows a broad peak around $2\theta = 20^o$ corresponding to 101plane of crystalline PVA [12] . Intensities of other peaks seen in the nano-ZnO, decrease in the XRD pattern of composite film, which signifies the crystallinity of PVA gets influenced by the presence of ZnO nanoparticles. It is also observed from Figure 2 that the strongest peak for Bragg's angle 36.2^0 is also present in the composite film indicating the presence of ZnO nanoparticles in the polymeric matrix.

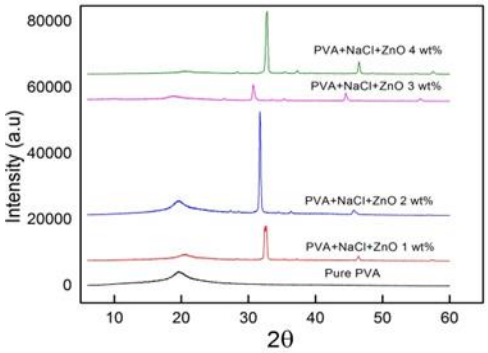

Figure 2. XRD pattern of Pure PVA and PVA/NAcl/ZnO nanocomposites.

Figure 4 shows simulated and experimental profiles for Pure PVA and PVA/ZnO Nano composites obtained with exponential column length distribution. The standard deviations in all the cases for the micro structural parameters are given in Table 1 as Δ. This Δ represents the statistical percentage of deviation of the parameters. The agreement between simulated and experimental intensity of the individual profiles in each of the samples are less than 10% of the mean value. With these parameters given in Table 1 as an input, we have further refined these parameters against whole pattern ($2\theta \approx 6^0$ to 60^0) recorded from the samples by taking summation which extends over the whole pattern [equation (6)]. We

have observed small but significant changes in these parameters with the set convergence of 1%. These changes are also given in Table 1. The goodness of the fit between simulated and experimental profiles for the samples were given in Figure 4.

The observed variation in the micro structural parameters given in Table 1 is due to a two-fold refinement. First we have carried out the line profile analysis of the extracted profiles from overlapping regions, which is a standard procedure to compute the micro structural parameters. Secondly, the range of overlapping regions determines the extent of broadening of the reflections. In fact, the broadening may decrease if the reflections are closer together and hence results in an increase in the crystallite size values. A closer look at the results in Table 1 and also the whole pattern indicates such a problem. It is

worth noting that none of other parameters, such as lattice strain and stacking fault probability, varied much during the refinement against the whole pattern data of the samples.

To check the reliability of the computed deformation and twin faults, we have used a simple approximate method suggested by Warren [18] and the expression for the twin fault is given by,

$$(2\theta^0_{CG} - 2\theta^0_{PM})_{hkl} = -14.6 X_{hkl} \tan\theta \; x \; \beta \qquad (8)$$

where $2\theta^0$ CG is the center of gravity of the Bragg reflection profile and $2\theta^0$PM is the peak maxima, β is the twin fault and X_{hkl} is the constant value, which we have taken to be 0.23. For all the samples we have computed the average twin fault probabilities are comparable to the values obtained by incorporating an appropriate expression in the Fourier coefficients. From this we would like to emphasize that these values are reliable and do represent the twin faults present in the sample in a direction perpendicular to the axis of sample. In fact, 1/β represents the number. We have also approximately estimated the deformation fault probability value α^d by making use of the following expression given by Warren [18],

$$\frac{1}{< D_S >} = \frac{1}{< D >} + [(1.5\alpha^d + \beta)/d_{hkl}]\,[\sum_b |L_0|/(u+b)h_0] \qquad (9)$$

where h_0=(h2+k2+l2)1/2 , u is the un broadened component, b is the broadened component and L_0=3N+1 reflections. A comparison with the deformation fault probability values obtained by

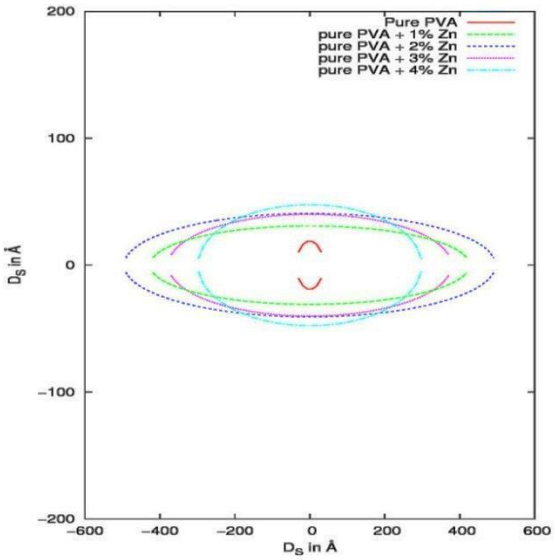

Figure 3: Variation of crystallite shape ellipsoid for Pure PVA and PVA/ZnO Nanoparticles

Fourier coefficient method (Table 1) indicates that the values are low, because there are too many layers between two successive deformation fault layers. This is due to the fact that there are pockets of crystalline like order in a matrix of amorphous regions. It is well known that the Fourier method gives a reliable set of micro structural parameters and we have shown that in addition to these values, one can also compute reliable fault probabilities. Also our investigation reveals that PVA/ZnO Nano composites have more Crystalline area than Pure PVA in PVA/ZnO Nano composites is greater than Pure PVA.Figure 3 a graphical plot of the crystallite shape ellipse reveals that the crystallite shape ellipse area increases as the concentration of ZnO nanoparticles increases in the Composite, The strength of the polymer samples is proportional to crystalline area, which is essentially equal to the area of ellipse

4. CONCLUSION

Whole X - ray pattern fitting procedure developed by us has been used to compute micro crystalline parameters. The stacking faults and twin faults for Pure PVA and PVA ZnO Nano composites nanoparticles are found to be very small. But as the concentration of the nanoparticles increases the Stacking faults and twin faults decreases due to nanoparticles loading as fillers into the polymer matrix.

Acknowledgements

Dr Mahesh acknowledges the encouragement and support of Management of MSRIT Bangalore, especially Department of Chemistry for their invaluable support in synthesis of Nanoparticles.

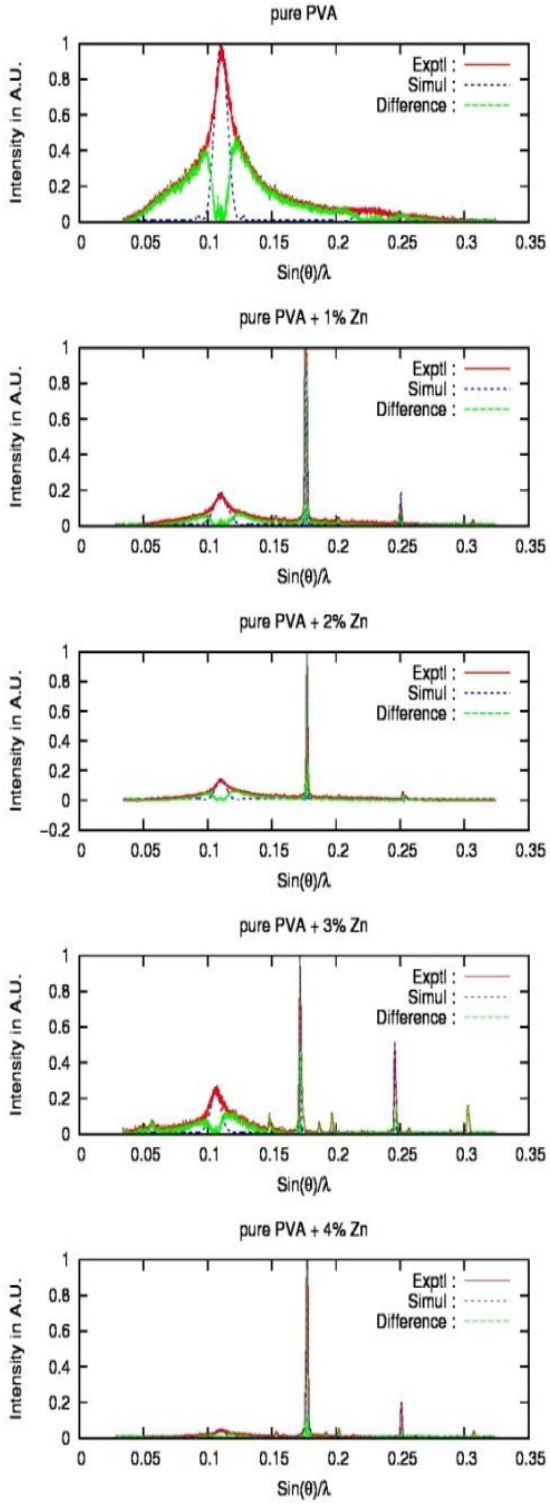

Figure 4. Simulated and experimental profiles for Pure PVA and PVA/ZnO nanocomposite.

5. REFERENCES

[1]. H. K. Feng Cheng, S. Nanda Gopal, Y. Pei Tan, Y. zheng Pan, H. qian Bao, L. Li, S. Hwa Chan, J. Zhao, (2012) Polyvinyl alcohol Nano-composites Filled with Poly(vinyl alcohol)-Grafted GrapheneOxide, *ACS **Applied . Mateial. Interfaces***, **4 (5)**, 2387-2394.

[2]. Regina Coeli Moreira Dias; Alfredo Miranda Góes, RogériaSerakides, ElianeAyres,Rodrigo Lambert Oréfice (2010) Porous Biodegradable Polyurethane Nanocomposites: Preparation, Characterization, and Biocompatibility Tests", ***Materials Research***,**13(2),**: 211-218

[3]. S. Morimune, M. Kotera, T. Nishino, K. Goto, K. Hata, (2011) Poly(vinyl alcohol) Nano-composites with Nanodiamond, ***Macro-molecules*, 44 (11)**, 4415-4421

[4]. M.R de Moura, R.J Avena-Bustillos, T.H McHugh, J.M Krochta, L.H Mattoso,(2008) Properties of novel hydroxypropyl methylcellulose films containing chitosan nanoparticles, ***Journal of Food Science***, **73(7)**, N31-7.

[5]. S. Elis Bianchi, V. Weiss Angeli, K. Cristinia Borgesdesouza, D. Santos Miron, G. de Almeida Carvalho, V. dos Sontos, R. Nichele Brandalise, (2011) Evaluation of the solubility of the HPMC/PVA blends in biological fluids in vitro , ***Material*, 14(2)**, 166-171.

[6]. N. Vorobyeva, M. Rumyantseva, D. Filatova, E. Konstantinova, D. Grishina., A. Abakumov, S. Turner, A. Gaskov, (2013) Nanocrystalline ZnO(Ga): Paramagnetic centers, surface acidity and gassensor properties ,***Sensors and Actuators B***, **182**, 555-564.

[7]. Al. Becheri, M. D. Pierandrea, L. Nostro, P. Baglioni, (2008) Synthesis and characterization of zinc oxide nanoparticles:application to textiles as UV-absorbers, ***Journal of Nanoparticle Research***, **10**, 679–689.

[8]. P. Judith, P. Espitia, N. de Fátima, F. Soares, J. S. d. Reis Coimbra, N. J. de Andrade, R. Souza Cruz, E. A. Alves Medeiros, (2012) Zinc Oxide Nanoparticles: Synthesis, Antimicrobial Activity and Food Packaging Applications, ***Food Bioprocess Technology***, **5**, 1447–1464.

[9]. Mohammed AzizIbrahem, Hung-YuWei, Meng-HungTsai, Kuo-ChuanHo, Jing-Jong Shyue, ChihWie Chu (2013) Solution-processed zinc oxide nanoparticles as interlayer materials for inverted organic solar cells, ***Solar Energy Materials & Solar Cells***, **108**, 156–163

[10]. K. Bajpai, Rashmi Gupta. (2011) Magnetically mediated release of ciprofloxacin from polyvinyl alcohol based superparamagnetic nanocomposites, ***Journal of Material Science: Mater Med*, 22**, 357–369.

[11]. Xiaomin Zhang, Jin Zhu, Xiaoqing Liu (2012) Preparation and Characterization of Regenerated Cellulose Blend Films Containing High Amount of Poly(vinyl alcohol) (PVA) in Ionic Liquid, ***Macromolecular Research***, **20**, 7, 703-708.

[12]. H. N. Chandrakala, B. Ramaraj, Shiva kumaraiah, G. M. Madhu, Siddaramaiah (2012) The influence of zinc oxide–cerium oxide nanoparticles on the structural characteristics and electrical properties of polyvinyl alcohol films ***Journal of Material Science*****, 47**:8076–8084.

[13]. M. Yousefi, E. Noori, D. Ghanbari, M. Salavati-Niasari, T. Gholami, (2013) A Facile Room Temperature Synthesis of Zinc Oxide Nanostructure and Its Influence on the Flame Retardancy of Poly Vinyl Alcohol**,** ***Journal of Cluster Science***, **DOI** 10.1007/s10876-013-0618-8

[14]. M. M. Ibrahim, W. K. El-Zawawy, M. A. Nassar (2010) Synthesis and characterization of polyvinyl alcohol/nanospherical cellulose particle films, ***Carbohydrate Polymers***,**79**, 694–699.

[15]. W. E Mahmoud, H M El-Mallah (2009) Synthesis and characterization of PVP-capped CdSe nanoparticles embedded in PVA matrix for photovoltaic application, ***Journal of. Physics. D: Applied. Physics*****, 42**, 035502 (5pp).

[16]. M. A. Kanjwala, F. A. Sheikhb, A.M Nasser . Barakatc, Xiaoqiang Li a,Hak Yong Kimc, Ioannis S (2012) Zinc oxide's hierarchical nanostructure and its photocatalyticproperties, ***Chronakisa, Applied Surface Science*****, 258**, 3695-3702

[17]. P Scardi, M. Leoni, (2002). Whole powder pattern modelling, ***Acta Crystallographica A*****, 58**, 190-200.

[18]. B E Warren (1969), X-ray Diffraction, (Addision-Wesley, New York).

[19]. R Somashekar, I H Hall, P D Carr (1989) The determination of crystal size and disorder from X-ray diffraction photographs of polymer fibres. 1. The accuracy of determination of Fourier coefficients of the intensity profile of a reflection, ***Journal of Applied Crystallography*****, 22**, 363-371.

[20]. B E Warren (1959), X-ray studies of deformed metals, ***Progress in Metal Physics,*** **8,** 147-202.